JOURNAL OF COLLOID AND INTERFACE SCIENCE **176,** 189–200 (1995)

Flocculation of Deformable Emulsion Droplets

I. Droplet Shape and Line Tension Effects

NIKOLAI D. DENKOV, DIMITER N. PETSEV,[1] AND KRASSIMIR D. DANOV

Laboratory of Thermodynamics and Physicochemical Hydrodynamics, Faculty of Chemistry, University of Sofia, 1126 Sofia, Bulgaria

Received September 28, 1994; accepted February 15, 1995

A simple theoretical model which allows the study of the configuration and the interaction energy of a doublet of flocculated Brownian droplets was recently proposed (Denkov *et al., Phys. Rev. Lett.* 71, 3226 (1993)). The model assumes that the doublet configuration consists of two deformed droplets having the shape of truncated spheres separated by a planar film. In this model the equilibrium film radius and thickness are determined by minimizing the total pair interaction energy which is presented as a sum of explicit expressions for the different contributions (van der Waals, electrostatic, steric, depletion, surface extension, etc.). In the present study this simplified model is numerically verified by comparison with the results stemming from the real shape of the interacting droplets. In order to determine the real configuration of two drops in contact we solve numerically the augmented Laplace equation of capillarity which accounts for the interaction between the droplets. Then the total interaction energy is alternatively calculated by integrating the energy density along the surfaces of the droplets. The numerical comparison shows that the equilibrium film radius and thickness, as well as the interaction energy calculated by means of the simplified model, are in very good agreement with the results from the more detailed (but more complex) approach. Numerical calculations of the equilibrium line tensions acting at the film periphery, as a function of the droplet radius, are performed. The obtained results are relevant also to flocs containing more than two particles since the theory predicts pairwise additivity of the interaction energy in most cases. The results can be useful in gaining a deeper understanding of the processes of stabilization or flocculation in emulsions.

Key Words: **emulsions, flocculation in; thin liquid film; line tension.**

1. INTRODUCTION

Emulsions are of great importance in many areas of human activity such as oil recovery and the food and beverage industry. From an academic viewpoint, they provide interesting and challenging problems, especially in relation to their stability against flocculation and coalescence. The stability of suspensions containing *solid particles* are usually treated in the framework of the Derjaguin–Landau–Verwey–Overbeek (DLVO) theory (1–3) which accounts for the electrostatic and van der Waals interactions between the particles. In the past decades it has been shown that other types of interparticle forces may also play an important role in the stability of dispersions—hydrodynamic interactions, hydration and hydrophobic forces, oscillatory structure forces, etc. (4, 5). It was proven both experimentally and theoretically that steric (6, 7) and depletion (8–10) interactions sometimes have a decisive effect on the dispersion stability.

The situation with *emulsions* is more complex (compared to that of suspensions of solid particles) due to the droplet fluidity and deformability. It is known that these two features may have a great impact on the hydrodynamic interactions and, hence, on the dynamic properties of such systems (11–16). They are particularly important for the kinetic stability of emulsions against coalescence (11–13). Along with the hydrodynamic interactions, the direct interactions due to surface forces can be strongly affected by the deformation (17–19). For that reason an approach to calculation of the different contributions (van der Waals, electrostatic, steric, depletion, etc.) to the interaction energy, when deformation takes place, was developed (20). It was assumed that the shape of two deformed drops in contact can be approximated with two truncated spheres separated by a planar film. A general explicit expression for the van der Waals interaction energy between two deformed droplets was derived (21) following the microscopic method of Hamaker (22). The contribution of the surface extension energy to the pair interaction potential was also appropriately included. It was shown that the stretching of the drop surface upon the deformation corresponds to a soft interdroplet repulsion. All the remaining possible interactions (electrostatic, steric, depletion, etc.) usually can be treated in the framework of Derjaguin's approximation (2, 3, 23), which allows for the two contributions of the total interaction energy: (i) across the flat film, and (ii) between the spherical surfaces surrounding the film (20).

[1] To whom correspondence should be addressed. E-mail: DimiterPetsev@Ltph.cit.bg.

0021-9797/95 $12.00

This approach was used elsewhere in a theoretical study of the coalescence phenomenon in emulsions (24). The processes of droplet deformation (film formation) and film thinning and rupture were included as consecutive stages in the general Smoluchowski (25) scheme of coalescence kinetics. In this case, the hydrodynamic interactions between deformable droplets were also included and the effect of surface fluidity was taken into account.

Some initial theoretical study of *flocculating but not coalescing* emulsion droplets was performed recently (26). In this paper the expressions for the energy contributions derived in Ref. (20) were used to calculate the equilibrium film thickness and radius, as well as the total interaction energy between two flocculated Brownian droplets of micrometer and submicrometer size (hereafter such a system is denoted as a *miniemulsion*). It was shown that the droplet deformation can strongly affect the pair interaction energy. In addition, a procedure for deriving the potential of mean force and the radial distribution function at low volume fractions (taking into account the droplet deformability) was formulated.

Still it remained unclear to what extent the *model droplet shape* assumed in Refs. (19–21, 24, 26) (two truncated spheres separated by a planar film) is correct. In the present paper we perform numerical calculations of the *actual shape* of two deformed droplets forming an equilibrium doublet (which presents also an independent interest). The augmented Laplace equation, which accounts for the interaction between the surfaces of the two droplets, is used for that purpose (27, 28). The energy of interaction between these droplets in equilibrium is determined (again numerically) by taking into account the real shape and is compared with the results from the model shape (truncated spheres). We show that the values of the interaction energy, the equilibrium film radius and thickness, calculated by means of the two approaches, are in very good agreement. This fact supports the accuracy of the numerical results and conclusions reported in Refs. (19–21, 24, 26). Furthermore, this finding allows us to perform numerical studies of emulsions consisting of deformable droplets on the basis of the much more simple (and less time consuming) computations involving the model shape rather than accounting for the actual one. Such numerical investigation of the effect of different factors (Hamaker constant, electrolyte concentration, interfacial tension, etc.) on the flocculation behavior of micrometer- and submicrometer-sized droplets is presented in the second part of this study (29). Another aim of the present paper is to specify a thermodynamic description of the system of two interacting deformable droplets. Such a treatment allows us to ascribe the components of the interaction energy between the droplets to appropriate thermodynamic quantities as disjoining pressure, film, line, and transversal tensions, etc., which are widely used in the thermodynamics of thin liquid films (2, 3, 27, 28).

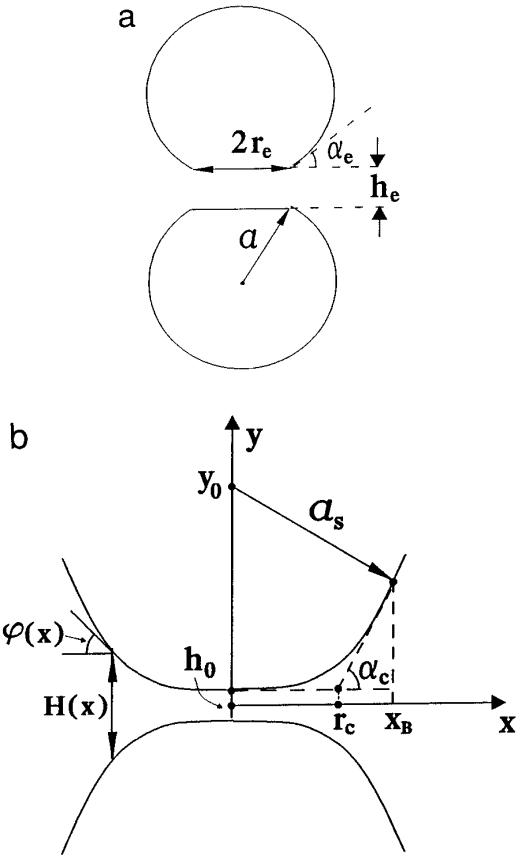

FIG. 1. Geometrical configuration of the system under consideration: (a) the simpler model of two droplets having the shape of spherical segments separated by a planar film—see Section 2.1; (b) sketch of the real shape where smooth transition between the planar film region and the spherical surfaces is present—see Section 2.2.

The structure of the paper is the following: In Section 2 the theoretical background is presented. It includes the determination of the equilibrium droplet shape (film radius and thickness) in the model and real systems, as well as the calculation of the pair interaction energy. Section 3 contains a numerical comparison of the droplet shape as determined from the two approaches. In Section 4 the different contributions to the interaction energy stemming from the two approaches are compared. The thermodynamic description of two interacting droplets and calculations of the line tensions acting at the film periphery are presented in Section 5. The conclusions are summarized in Section 6.

2. THEORETICAL BACKGROUND

2.1. Configuration of the Idealized System

In accordance with the model proposed in Refs. (20, 26) we assume that the two droplets have the shape of spherical segments separated by a planar film—see Fig. 1a. The droplet separation is characterized by the film thickness, h_e, and

the deformation by the film radius, r_e. The indexes ''e'' mean equilibrium values. Since only small deformations are considered, $(r_e/a)^2 \ll 1$, it is shown (20, 26) that the radius of curvature of the spherical segments, a, is practically the same as of nondeformed spherical droplets of the same volume (the actual difference is a higher order correction). For simplicity we restrict our consideration to the case of equal in size and interfacial tension droplets. A generalization to the case of two different drops (or to the interaction between a droplet and a flat interface) is possible (20).

According to the approach developed in Refs. (20, 26), the interaction energy between the drops can be expressed as

$$W(h, r) = W^{VW} + W^{S} + \Delta W. \qquad [2.1]$$

The first contribution term to the total interaction potential, $W(h, r)$, is the van der Waals energy (20) [cf. also Ref. (21)]

$$\begin{aligned} W^{VW}(h, r) &= -\frac{A_H}{12}\left\{\frac{2al}{(l+h)^2} + \frac{2al}{h(2l+h)} + 2\ln\left[\frac{h(2l+h)}{(l+h)^2}\right]\right. \\ &\quad + \frac{r^2}{h^2} - \frac{2r^2}{h(l+h)} - \frac{2r^2}{(l+h)[2(l-a)+h]} \\ &\quad + \frac{(h^2+4r^2)(\sqrt{h^2+4r^2}-h)}{2h[2(l-a)+h]^2} \\ &\quad \left. - \frac{2r^2a(2l^2+lh+2ah)}{h(l+h)^2[2(l-a)+h]^2}\right\}, \end{aligned} \qquad [2.2]$$

where $l = a + \sqrt{(a^2 - r^2)}$, and A_H is the Hamaker constant. (Note that in the last term of Eq. [3.14] in Ref. (20) a multiplier a was omitted.) In Ref. (20) a more general expression for the van der Waals interaction between two different in size truncated spheres (or between a truncated sphere and an infinite flat wall) was derived.

The surface dilational energy, W^S, accounts for the increase of the interfacial energy during the deformation. For small deformations it can be approximated with the expression (19, 20)

$$W^S(r) = \gamma\frac{\pi}{2}\frac{r^4}{a^2}, \quad \text{for } \left(\frac{r}{a}\right)^2 \ll 1, \qquad [2.3]$$

with γ being the interfacial tension of nondeformed droplets. The surface dilational energy may depend in some cases on the Gibbs elasticity of the adsorbed monolayer. The expression containing this contribution is given by Eq. [3.25] in Ref. (20) [cf. also Ref. (24)].

ΔW stands for other types of interdroplet interactions which usually can be evaluated in the framework of Derjaguin's approximation (2, 3, 20, 23)

$$\Delta W(h, r) = \pi r^2 f(h) + \pi a\int_h^\infty f(H)\,dH, \quad \text{for } \frac{h}{a} \ll 1, \left(\frac{r}{a}\right)^2 \ll 1, \qquad [2.4]$$

where $f(h)$ denotes the interaction energy per unit area in an infinite flat film of thickness h. The term proportional to r^2 in Eq. [2.4] corresponds to the interaction across the planar film, while the remaining term accounts for the interaction between the spherical surfaces surrounding the film. It is important to note that at small deformations *the contributions of these two terms in the total interaction energy are usually comparable.* Most of the interparticle interactions (such as electrostatic, steric, hydrophobic, or hydration) can be often expressed as exponential functions (4)

$$f(h) = B\exp\left(-\frac{h}{\sigma}\right), \qquad [2.5]$$

where the parameter σ determines the range of the interaction. The parameter B is positive for repulsive interactions and negative for attractive ones. The explicit expressions for B and σ depend on the specific interaction under consideration. For instance, the electrostatic interaction between two deformed drops can be evaluated by means of Eqs. [2.4] and [2.5] with σ being equivalent to the Debye screening length κ^{-1}. For z:z electrolyte κ is defined as

$$\kappa^2 = \frac{2e^2z^2}{\epsilon_0\epsilon kT}C_{EL}, \qquad [2.6]$$

where e is the elementary charge, ϵ is the relative dielectric permittivity of the medium, ϵ_0 is dielectric permittivity of free space, kT is the thermal energy, and C_{EL} is the electrolyte concentration. In the framework of the so-called ''nonlinear superposition approximation'' (1, 6) B is given by the expression

$$B = 64\,C_{EL}kT\kappa^{-1}\tanh^2\left(\frac{ze\Psi_0}{4kT}\right), \qquad [2.7]$$

where Ψ_0 is the droplet surface potential.

For the steric interaction more rigorous (and complex) expressions for $f(h)$ are available (4–7; 29, Sect. 4.3; 30–32). Other important exceptions which do not obey Eq. [2.5] are the depletion and oscillatory interactions due to the presence of much smaller colloid particles (micelles or polymer molecules) in the disperse medium (4, 8–10, 26,

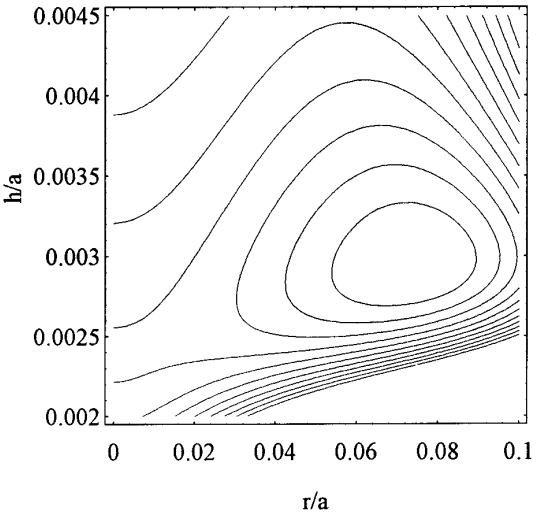

FIG. 2. Contour-plot of the total pair interaction energy, W (calculated as explained in Section 2.1), as a function of the film thickness, h, and film radius, r. The parameters are radius of the nondeformed droplets $a = 2\ \mu$m, interfacial tension $\gamma = 1$ mN/m, Hamaker constant $A_H = 10^{-20}$ J, electrical surface potential $\Psi_0 = 100$ mV, electrolyte concentration $C_{EL} = 0.2$ M. The distance between two contours equals 10 kT. The minimum $W_e/kT = 109.7$.

33–36). They are discussed in Sections 4.1 and 4.2 of the second part of this study (29).

The combination of Eqs. [2.1]–[2.4] (with a particular form of $f(h)$ depending on the type of interactions involved) allows the calculation of the interaction energy, W, as a function of the interdroplet separation (characterized by the film thickness, h) and of the droplet deformation (characterized by the film radius, r). The resulting potential surface, $W(h, r)$, can have complex shape when several types of interactions are simultaneously operative. Usually at least three interactions are acting together between two deformable drops: (i) the long range van der Waals interaction, (ii) the surface extension energy which corresponds to a soft repulsion and restricts the increase of the film radius, and (iii) some short range repulsion (electrostatic and/or steric) which prevents the film rupture. In addition, the presence of smaller colloidal species (micelles, polymer molecules) can cause depletion or oscillatory interaction at separations comparable with their diameter. Therefore, the function $W(h, r)$ may have one or several (or no) local minima, which can be analyzed by means of standard mathematical procedures. An illustrative way to present $W(h, r)$ is to use a contour-plot (or three-dimensional plot)—see Fig. 2. The specific *equilibrium* values of r and h for given parameters (Hamaker constant, electrical surface potential, ionic strength, interfacial tension, etc.) are calculated for the minimum of the total interaction energy, $W_e = \min\{W(r, h, a)\}$. One should note that in reality h and r can fluctuate around their equilibrium values. In an equilibrium ensemble of droplets the probability of finding a pair of drops in a configuration with given h and r is proportional to $\exp[-W(h, r)]$. Since in the present study we are primarily interested in time averaged properties of the system, we neglect these fluctuations. For definiteness hereafter we call ''equilibrium'' the values of h and r corresponding to a minimum of the function $W(h, r)$, denoting them h_e and r_e.

As shown in Ref. (26) one can determine the radial distribution function of the system, $g(z)$, (at low volume fractions) by means of the expression

$$g(z) = \frac{4}{\Gamma(1/4)} \left(\frac{\pi a^2 \gamma}{2kT} \right)^{1/4} \frac{1}{a} \int \exp\{-W[h(r), r]/kT\}\, dr, \qquad [2.8]$$

where z is the distance between the mass centers of the drops and $\Gamma(x)$ is the gamma function of Euler. Note that a given z can be realized with a set of values of r and h. The integration in Eq. [2.8] is performed over all possible configurations of the doublet of droplets providing a given distance z (26). The normalization multiplier in Eq. [2.8] is determined in such a way to ensure $g(z \to \infty) = 1$. The radial distribution function can be used to study the statistical-mechanical properties of ensembles of deformable Brownian droplets, like osmotic pressure, phase behavior. A method for producing emulsions containing such small and monodisperse droplets of micrometer and submicrometer size was recently developed by Bibette *et al.* (37).

2.2. *Configuration of the Real System*

In order to describe the real shape of two droplets in contact one should solve numerically the Laplace equation of capillarity taking into account the interaction between the droplets. As shown previously (27, 28) for not-too-small droplets the interaction can be taken into account by introducing the concepts of disjoining pressure, $\Pi(H)$, and variable interfacial tension, $\gamma(H)$, where $H(x)$ is the local film thickness—see Fig. 1b. This approach is applicable when the interaction is of range much smaller than the droplet radius and one can use the general form of the Derjaguin approximation (3), i.e., to assume that $\Pi(H)$ is approximately the same as for an infinite planar film of thickness H,

$$\Pi(x) = \Pi[H(x)]. \qquad [2.9]$$

In this case the interfacial shape, $H(x)$, can be determined from the system of three equations (27, 28)

$$\frac{d(\gamma \sin \phi)}{dx} + \frac{1}{x}\gamma \sin \phi = P_c - \Pi(x) \qquad [2.10]$$

$$\frac{dH}{dx} = 2 \tan \phi \qquad [2.11]$$

$$\frac{d\gamma}{dx} = -\Pi(x) \sin \phi \qquad [2.12]$$

for the three unknown functions $H(x)$, $\phi(x)$, and $\gamma(x)$ if $\Pi(x)$ is known. Here $\phi(x)$ describes the running slope angle of the interface and P_c is the capillary pressure. The system [2.10]–[2.12] ensures the following limiting cases:

(i) At large separations between the surfaces of the droplets, the interaction becomes negligible, $\Pi \to 0$, and for P_c = const, Eqs. [2.9]–[2.11] predict a spherical shape of the interface. In this region $\gamma = \gamma^1$ = const (cf. Eq. [2.12]) and γ^1 is the interfacial tension in the regions where the interaction is negligible (in the present study we assume that γ^1 is equal to the interfacial tension of the nondeformed drops, γ).

(ii) In the central zone ($x \to 0$) $\sin\phi$ is very small. This corresponds to an (almost) flat portion of the interface, which is approximated in the simpler model approach (subsection 2.1) with planar film. Here $\gamma = \gamma^f \approx$ const and γ^f is the film surface tension which, in general, is different from γ^1 (see Eq. [5.1] below).

In this way the set of Eqs. [2.10]–[2.12] provides a smooth transition from an almost planar film of thickness h_0 (Fig. 1b) to a spherical surface which is not perturbed by the interaction far from the contact region. In the framework of this description, the thermodynamic film radius, r_c, is defined as the crossection of the extrapolated spherical surface with the plane $H = h_0$ (27, 28). We stress here that the notations h_0 and r_c mean film thickness and film radius in the framework of the approach based on the augmented Laplace equation, while h_e and r_e refer to the model truncated sphere shape.

In order to solve numerically Eqs. [2.10]–[2.12], we need to specify three boundary conditions for the unknown functions. It is convenient to start the numerical integration from a point x_B which corresponds to large local intersurface separation (Fig. 1b). Due to the negligible interaction in this region, the interface has a spherical shape which is characterized by its radius, a_s, and its geometrical center, y_0. Note that $a_s \geqslant a$ (a is the radius of nondeformed spherical droplets of the same volume). Once a_s and y_0 are specified (see below) one can start the numerical integration with the following boundary conditions:

$$H_B \equiv H(x_B) = 2(y_0 - \sqrt{a_s^2 - x_B^2}) \qquad [2.13]$$

$$\tan \phi(x_B) = \frac{x_B}{\sqrt{a_s^2 - x_B^2}} \qquad [2.14]$$

$$\gamma(x_B) = \gamma^1 + \frac{1}{2} f(H_B). \qquad [2.15]$$

The interaction energy per unit area, $f(h)$, in an infinite flat film of thickness h is related to the disjoining pressure through the expression

$$f(h) \equiv \int_h^\infty \Pi(H) dH. \qquad [2.16]$$

Equations [2.13] and [2.14] are geometrical relationships accounting for the spherical shape in this region. Equation [2.15] is strictly applicable only for a planar film, but can be used in the present case as far as the slope angle at the point x_B is small and the Derjaguin approximation is justified (27, 28).

In order to determine the geometrical parameters which characterize the spherical surface, y_0 and a_s, we used the following two conditions. Since the fluids are incompressible, we know the total volume of the droplet,

$$V = \frac{4}{3}\pi a^3 = \frac{1}{2}\int_{h_0}^{H_B} \pi x^2(H) dH + \frac{\pi p^2 (3a_s - p)}{3},$$

$$p = a_s + \sqrt{a_s^2 - x_B^2}. \qquad [2.17]$$

Here a is the radius of nondeformed drops and $x(H)$ is the function describing the drop shape in the region $\frac{1}{2} h_0 \leqslant y \leqslant y_B$. Another condition stems from the requirement of mechanical equilibrium of the doublet. In the absence of outer forces this corresponds to the restriction

$$F = \int_{x=0}^{x_B} \Pi(x) 2\pi x dx = 0, \quad \text{at equilibrium.} \qquad [2.18]$$

The following numerical procedure was used. Initial values of y_0 and a_s are prescribed (we used $y_0 = a_s = a$). The system [2.10]–[2.12] with boundary conditions [2.13]–[2.15] is integrated (using a Runge–Kutta scheme) to determine the first approximation to the interfacial shape in the region $x_B \geqslant x \geqslant 0$. The remaining portion of the interface is assumed to be spherical with radius a_s. Then the condition, Eq. [2.18], is checked. If $F < 0$ (which corresponds to net interdroplet attraction) the value of y_0 is reduced and vice versa. Simultaneously a new value of a_s is ascribed from the numerical solution of Eq. [2.17]. The new values of y_0 and a_s are used for determination of the subsequent approximation of the interfacial shape. The integration procedure is repeated until such values of y_0 and a_s are found which simultaneously satisfy Eqs. [2.17] and [2.18]. We should emphasize that this procedure is extremely sensitive with respect to the initial value of y_0 (due to the nonlinearity of Eqs. [2.10]–[2.12]) and requires very small steps to be

used, otherwise the solution could be missed and the numerical procedure may become divergent. If carefully applied, the procedure is convergent and provides the unique solution of all set of equations [2.10]–[2.18].

Once the droplet shape is determined, one can proceed with the calculation of the different components of the interaction energy. The surface extension energy is proportional to the area increase upon deformation:

$$W^{s} = 2\gamma\left[2\pi \int_0^{x_B} x\sqrt{1 + \tan^2 \phi(x)}\, dx + 2\pi a_s p - 4\pi a^2 \right]. \quad [2.19]$$

The remaining components are calculated by means of the Derjaguin approximation (3)

$$W^{VW} = 2\pi \int_0^{x_B} x\sqrt{1 + \tan^2 \phi(x)} \left[-\frac{A_H}{12\pi H^2(x)} \right] dx \quad [2.20]$$

$$W^{EL} = 2\pi \int_0^{x_B} x\sqrt{1 + \tan^2 \phi(x)}\, [B \exp(-\kappa H)]dx, \quad [2.21]$$

where B and κ are given by Eqs. [2.6] and [2.7].

The calculations show that the obtained interfacial shapes (and interaction energies) depend slightly on the value of x_B if the latter lies in the interval $0.35 < x_B/a < 0.5$. The points in this region satisfy simultaneously the two requirements: (i) negligible interaction between the drop surfaces (large separation, H) and (ii) small meniscus slope, $\sin^2\phi \ll 1$. However, for small drops (e.g., of radius smaller than 2 μm) these two conditions can not be satisfied at the same time and this approach cannot be applied. The main reason for this problem is the very long range of van der Waals interactions which cannot be satisfactorily described by Derjaguin approximation for small drops. It is possible in principle to avoid the use of any approximations in the calculations of the VW interaction by using a numerical approach for obtaining the interaction between two axisymmetrycal bodies with arbitrary profiles (20). One should bear in mind, however, that this calculation has to be combined with the determination of the actual droplet profile from the Laplace equation which leads to enormous computational difficulties. Still we performed some calculations using this very heavy but exact procedure and found that above 2 μm, the approximate consideration of the van der Waals interactions could be used without lack of accuracy. Hence for extensive numerical calculations we used the approach based on the approximate consideration of the van der Waals interactions which is much simpler and less time consuming. On the other hand, the approximate model approach described in Section 2.1, Eq. [2.2], can be applied for much smaller droplets because the van der Waals interaction is calculated *exactly* for the assumed geometry (i.e., the Derjaguin approximation is not used in this case). Therefore, numerical comparison between the two approaches is performed only for droplets of micrometer size or even larger.

3. COMPARISON OF THE INTERFACIAL SHAPE IN THE REAL AND IDEALIZED SYSTEMS

The *model droplet shape* in the idealized system (truncated spheres) is characterized by three geometrical quantities determined by minimization of the pair interaction energy as explained in Section 2.1: the spherical segment radius, a (which is practically equal to the radius of the nondeformed droplets—see below), the film radius, r_e, and the film thickness, h_e. One can also define the equilibrium film–meniscus contact angle (see Fig. 1a) through the relationship

$$\alpha_e = \arcsin (r_e/a). \quad [3.1]$$

The contact angle is a quantity which is often used in the thermodynamic description of thin liquid films for characterizing the interaction energy (see Section 5).

On the other hand, the *real shape* is completely characterized by the function $H(x)$ determined in accordance with the procedure described in Section 2.2. For comparison with the model system one can use the thermodynamic film thickness, h_0, and radius, r_c. These quantities correspond to h_e and r_e in the model approach, respectively. The thermodynamic contact angle, α_c, (which should be compared with the contact angle in the model approach, α_e) is found from a counterpart of Eq. [3.1],

$$\alpha_c = \arcsin(r_c/a_s). \quad [3.2]$$

In Fig. 3 we compare the calculated profile of the droplets in the region of contact (the full curve) with the model shape (the dashed curve). The interactions taken into account are surface extension, van der Waals, and electrostatic (see Eqs. [2.1]–[2.7] and [2.10]–[2.21]). The parameters of the droplets used in these calculations are radius of the nondeformed droplets $a = 2$ μm, interfacial tension $\gamma = 1$ mN/m, Hamaker constant $A_H = 10^{-20}$ J, electrical surface potential $\Psi_0 = 100$ mV, and electrolyte concentration $C_{EL} = 0.2$ M. One sees from the figure that the agreement between the curves is very good. In particular, a thermodynamic film thickness $h_0 = 5.86$ nm, versus model film thickness, $h_e = 5.92$ nm, was determined. For the thermodynamic film radius and contact angle we obtained $r_c = 161.9$ nm and $\alpha_c = 4.64°$, while for the respective values from the model approach we

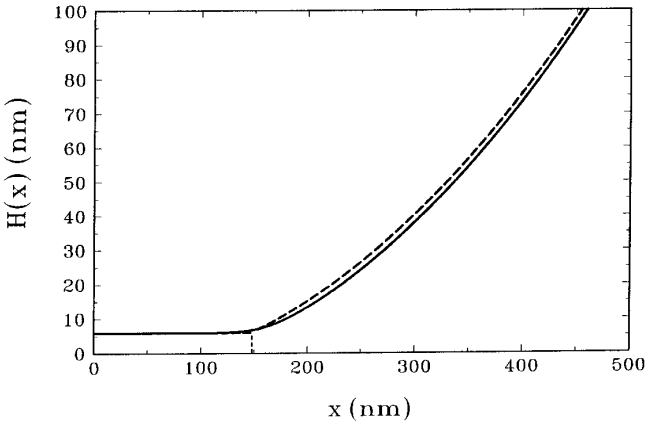

FIG. 3. Comparison of the droplet shape determined by the two approaches. The full curve represents the droplet shape obtained by numerical integration of Laplace equation of capillarity (Section 2.2). The dashed curve represents the simpler model shape (spherical segments separated by a planar film) with film thickness and radius calculated as explained in Section 2.1. The parameters are the same as those in Fig. 2.

calculated $r_e = 147.8$ nm and $\alpha_e = 4.24°$. The calculations showed that the radius of curvature of the spherical droplet surface increases very slightly upon the deformation: $a_s = 2.0000066$ μm. Therefore, the use of the radius of the nondeformed droplets, a, when calculating the interaction energy between two deformed droplets (see Eq. [2.4]) is justified.

Comparison of the film thickness and radius, and three-phase contact angle obtained by the numerical (h_0, r_c, and α_c) and model (h_e, r_e, and α_e) approaches is presented in Table 1 and Fig. 4 for droplets of radii between 1 and 10 μm. As seen in the table, the results are in a rather good agreement. The model values of the film radius and contact angle are slightly smaller than the numerical ones. This fact is connected with the presence of negative line tension, χ in the numerical approach (see the last column in the table), which takes into account the difference between the actual and model shapes. As discussed in Section 5, in the model approach the line tension is identically zero. The film radius calculated by means of the model approach (26) sharply decreases for submicron droplets due to the increased capillary pressure. This effect is analyzed in detail in the framework of the model approach in the second part of this study (29). The slight rise of the dimensionless film radius obtained by solving the Laplace equation (full curve) may be due to a numerical inaccuracy for small droplets connected with the long range of the van der Waals interactions (see the discussion at the end of subsection 2.2). We did not make comparison for *submicrometer* droplets because of the same reason.

4. COMPARISON OF THE INTERACTION ENERGIES CALCULATED BY MEANS OF THE TWO APPROACHES

The total interaction energy is an important quantity which determines many equilibrium and nonequilibrium properties of the system. In the present study we discuss only the interaction energy in an equilibrium doublet of droplets in the absence of outer force. Note that for small deformations of the droplets, $(r/a)^2 \ll 1$, the interaction energy is additive and many of the conclusions can be applied to multiparticle interactions appearing in flocs of droplets. The case when an outer force (e.g., gravity) is present along with the surface forces is described in a separate study (38), where the interaction between a fluid particle (droplet, bubble) and a fluid interface is considered in detail.

It is instructive to compare not only the total interaction energy but also the values of its components. For deformable droplets like those shown in Fig. 3, one has three contribu-

TABLE 1

Comparison of the Results Obtained by the Approach Based on (i) the Numerical Integration of the Augmented Laplace Equation Presented in This Paper and (ii) the Model Approach (Postulated Shape of Spherical Segments) Developed in Ref. (26)

a	W/kT		W^{VW}/kT		W^{EL}/kT		W^{S}/kT		h_0 [nm]	h_e [nm]	r_c [nm]	r_e [nm]	α_c	α_e	$\tau \times 10^2$ [mN/m]		$\chi \times 10^{13}$ [N]
μm	(i)	(ii)	(i)	(ii)	(i)	(ii)	(i)	(ii)	(i)	(ii)	(i)	(ii)	(i)	(ii)	(i)	(ii)	(i)
1	−46.9	−42.6	−70.7	−65.0	12.4	11.6	11.3	10.8	5.65	5.78	84.2	72.9	4.83°	4.18°	8.42	7.29	−0.95
2	−117.5	−109.7	−200.0	−192.1	37.6	36.8	44.8	45.6	5.86	5.92	161.9	147.8	4.64°	4.24°	8.10	7.39	−1.13
3	−210.6	−200.4	−386.3	−379.9	75.4	75.5	100.3	103.9	5.95	5.97	237.8	222.4	4.55°	4.25°	7.93	7.41	−1.23
4	−325.9	−314.7	−629.4	−628.2	125.8	127.8	177.8	185.8	6.00	5.98	312.8	297.0	4.48°	4.26°	7.82	7.42	−1.31
5	−463.5	−452.4	−929.5	−947.0	188.7	195.7	277.2	298.9	6.03	6.02	387.3	373.9	4.44°	4.29°	7.75	7.48	−1.37
6	−623.3	−613.7	−1286.3	−1315.1	264.3	274.6	398.8	426.7	6.06	6.03	461.6	447.8	4.41°	4.28°	7.69	7.46	−1.42
7	−805.2	−798.6	−1700.1	−1739.5	352.5	366.1	542.3	574.8	6.07	6.04	535.7	521.0	4.39°	4.27°	7.65	7.44	−1.46
8	−1009.4	−1006.9	−2170.6	−2229.5	453.3	472.3	708.0	750.3	6.09	6.04	609.6	593.6	4.37°	4.26°	7.62	7.42	−1.50
9	−1235.7	−1238.6	−2698.0	−2748.3	566.6	584.7	895.7	925.0	6.10	6.05	683.4	665.4	4.36°	4.24°	7.61	7.39	−1.54
10	−1484.2	−1493.6	−3282.4	−3327.5	692.8	710.7	1105.4	1123.2	6.11	6.05	757.1	736.3	4.34°	4.22°	7.57	7.36	−1.57

Note. The droplet parameters are $A_H = 10^{-20}$ J, $\gamma = 1$ mN/m, $C_{EL} = 0.2$ M, $\Psi_0 = 100$ mV.

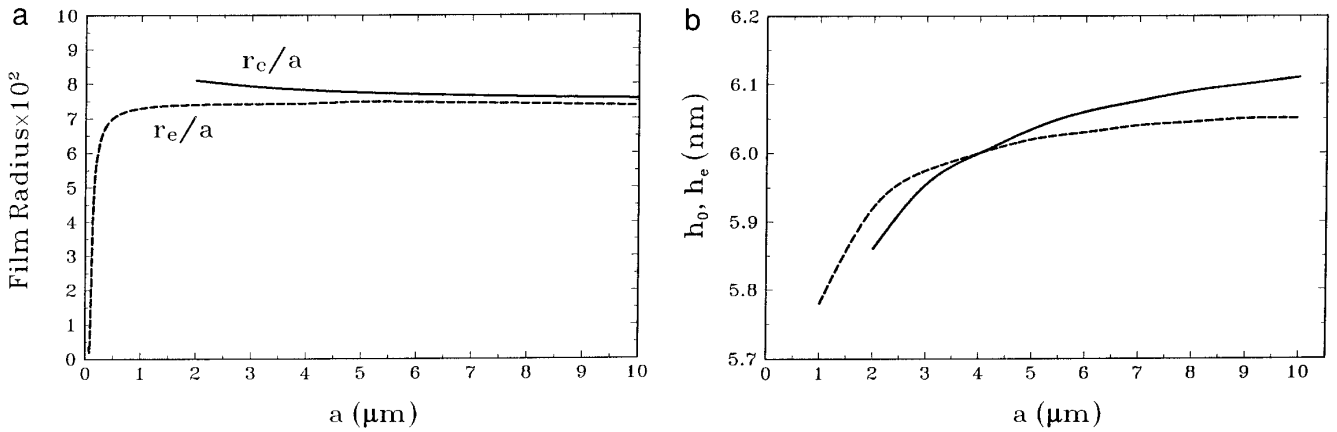

FIG. 4. Dimensionless film radius (a) and film thickness (b) as functions of the droplet radius. The remaining parameters used in the calculation are the same as in Fig. 2. r_c and h_0 correspond to the thermodynamic film radius and thickness while r_e and h_c correspond to the model approach.

tions to the energy—van der Waals, electrostatic, and surface extension. For such droplets (of radius $a = 2$ μm—see Table I) we calculated from the real shape the following values: $W^{VW}/kT = -200$, $W^{S}/kT = 44.8$, and $W^{EL}/kT = 37.6$. The respective values from the model shape are $W^{VW}/kT = -192.1$, $W^{S}/kT = 45.6$, and $W^{EL}/kT = 36.8$. The comparison shows that the van der Waals interaction calculated from the simpler model shape of the droplets is slightly underestimated (the relative error is about 4%). The other two contributions are calculated more accurately (relative error about 2%). As a final result, for the total interaction energy we calculate $W/kT = -117.5$ using the real drop shape and $W_e/kT = -109.7$ using the simple model. This makes a relative error of 7.1%.

As seen from the results presented in Table 1, one may have an important contribution from the surface extension when the interaction energy between two deformed droplets is considered. Its relative contribution to the total interaction potential can be very important and, as seen from the calculations, can be comparable to (and even larger than) the electrostatic repulsion. Physically, the surface extension energy corresponds to a soft repulsion between the droplets which tends to restrict the growth of the planar film.

In Fig. 5 we compare the total interaction energy calculated by the two models for droplets of radii between 1 and 10 μm. The solid curve is calculated from the actual droplet shape (Section 2.2) while the dashed curve corresponds to the simpler model approach described in Section 2.1. Although theoretical, the two approaches are subject to certain restrictions and approximations. These approximations and restrictions are the reason for the discrepancy between them. The approach based on the idealized geometry bears the disadvantages of implying artificially a shape of a truncated sphere, while the approach using the Laplace equation bears the problem with the van der Waals interactions in the framework of the Derjaguin approximation and is questionable around 1 μm sized droplets. Above 2 μm, however, it was shown to be accurate enough (see subsection 2.2). The discrepancy between the two approaches is due mainly to the artificial shape in the approach based on the idealized geometry. As seen from the figure and the table, the agreement is very good in the whole range of radii studied—the relative error is less than 10% and sharply decreases with increased droplet size. The results stemming from the two approaches are compared in Table 1. As seen in the table, the different contributions to the interaction energy also agree very well for the whole range of droplet radii studied.

In order to analyze the forces acting in the film region we present in Fig. 6 the disjoining pressure, Π, as a function of the film thickness, h, and of the radial coordinate, x. The parameters are the same as in Fig. 3. The plot of $\Pi(h)$ (Fig. 6a) is typical for the interplay of DLVO forces—van der Waals attraction at larger distances and electrostatic repulsion at small distances. The deep minimum at very small separation, when the van der Waals forces are divergent and

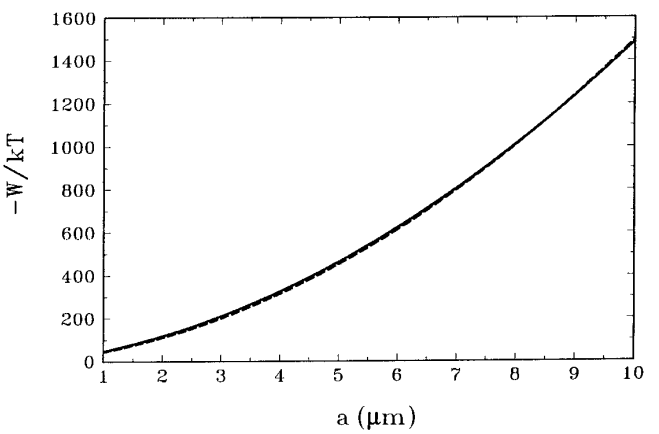

FIG. 5. Interaction energy vs droplet radius. The full curve corresponds to the result obtained by solving the augmented Laplace equation and the dashed curve to the model approach. The parameters are the same as those in Fig. 2.

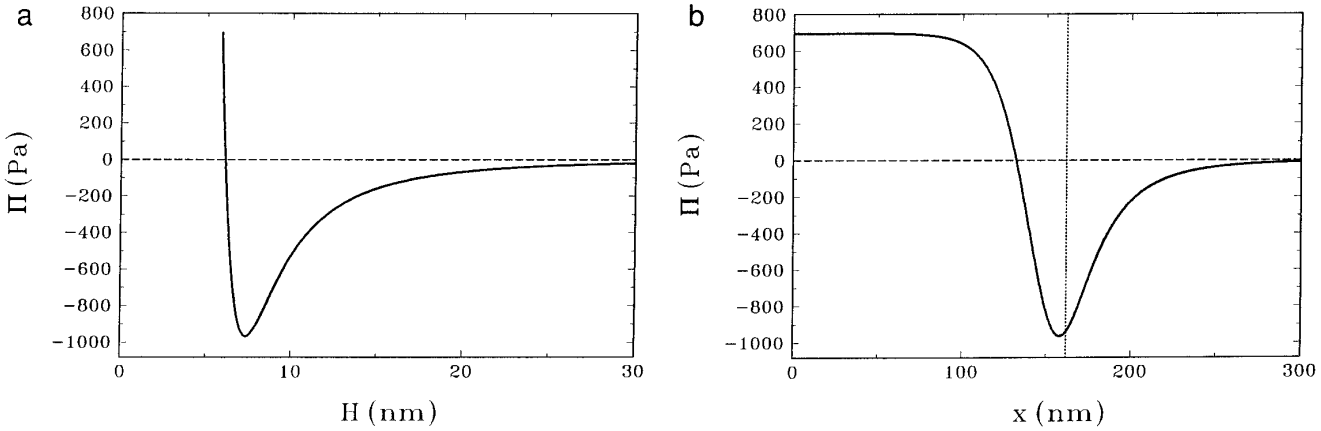

FIG. 6. Plot of the disjoining pressure Π as a function of (a) the surface-to-surface separation H (for flat interacting surfaces), and (b) the radial coordinate x, i.e., the pressure profile along the film radius. The parameters are the same as those in Fig. 2 and the coordinates correspond to those specified in Fig. 3. The vertical dashed line in (b) denotes the thermodynamic film radius.

strongly predominate, is not shown in the figure. The plot of the function $\Pi(x)$ presented in Fig. 6b shows that the droplets repel each other (the electrostatics prevails) in the film region, while the van der Waals attraction dominates in the regions around the film. Therefore, *the attachment of the droplets is due to the attraction between the spherical surfaces around the film* (5) and not to the interaction across the film. This means that the equilibrium can not be explained without accounting for the interaction between the surfaces around the film. In the thermodynamic description this is taken into account by introducing the so-called ''transversal tension,'' τ (27, 28). The net interaction force (integrated throughout the droplet surfaces) is zero in this case as imposed by Eq. [2.18].

5. THERMODYNAMIC DESCRIPTION OF THE DOUBLET OF DROPLETS. LINE AND TRANSVERSAL TENSIONS

5.1. General Thermodynamic Relationships

The thermodynamics of thin liquid films is very well developed and described in the literature. For reviews the reader can refer to (3, 5, 28, 39). We follow the so-called ''detailed approach'' which is most convenient when the interaction between the film surfaces is considered (5, 28, 39–41). According to it, the liquid film consists of a phase which is identical to that of a disperse medium sandwiched between two Gibbs film surfaces of zero thickness (see Fig. 7). The interaction between the film surfaces is accounted for by the disjoining pressure (force per unit area), Π, or by the free interaction energy per unit area, f, which are interrelated by means of Eq. [2.16]. The tension of the film surfaces, γ^{f}, is different from the tension of the single interface, γ^{l}, due to the interaction between the droplets,

$$\gamma^{f}(h) = \gamma^{l} + \frac{1}{2}\int_{h}^{\infty} \Pi(h')dh' = \gamma^{l} + \frac{1}{2} f(h). \quad [5.1]$$

Other important characteristics of the film are its thickness, radius, and contact angle, which can be determined experimentally in many cases. From these quantities one can obtain information about the equilibrium disjoining pressure and interaction energy due to the relationships (27, 28)

$$\Pi(h) = P_c, \text{ at equilibrium} \quad [5.2]$$

$$\gamma^{f} = \gamma^{l} \cos \alpha_c - \frac{\chi}{r_c}, \quad [5.3]$$

where χ is called line tension. As shown in Refs. (27, 28) Eq. [5.3] is equivalent to a force balance at the film periphery in the direction tangential to the contact. The force balance in normal direction is provided by the *transversal* line tension, τ, introduced by Kralchevsky and Ivanov (27):

$$\tau = \gamma^{l} \sin \alpha_c. \quad [5.4]$$

In fact the line and transversal tensions are linear counterparts of the surface tension and disjoining pressure (27). In

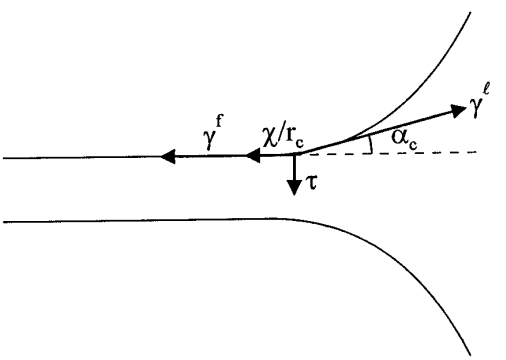

FIG. 7. Sketch of the film–meniscus transition region.

particular, τ can be expressed as a linear excess of the disjoining pressure,

$$\tau = \frac{1}{r_c}\int_0^{x_B} [P_c\,\Theta(r_c - x) - \Pi(x)]x\,dx, \qquad [5.5]$$

where x_B denotes a point which corresponds to very large separation of the film surfaces (negligible interaction—see subsection 2.2 and Fig. 1b), P_c is the capillary pressure, and $\Theta(x)$ is the Heaviside function

$$\Theta(x) = 0, \quad \text{for } x < 0$$
$$\Theta(x) = 1, \quad \text{for } x > 0. \qquad [5.6]$$

These general considerations are also valid in the case of thin films formed between two deformed droplets like those shown in Fig. 1.

5.2. Line and Transversal Tensions

Although a number of papers have been published dealing with the theoretical calculation (42–44) and experimental measurement (45–49) of the line tension χ (or similar quantities related to χ), the value and even the sign of χ are subject to much discussion in the literature. The experimental difficulties are connected with the need for very precise measurement of the variation of the three-phase contact angle with the film radius under well defined conditions (see Eq. [5.3]). In some studies very large values (of the order of 10^{-7} N or even larger) of the line tension were measured (45–48) with drops on solid surfaces or with small bubbles attached to water surface. These large values are usually explained as a result of some dynamic nonequilibrium effects (46–48). On the other hand, the theoretical calculations of χ usually predict equilibrium values which are several orders of magnitude smaller (42).

The system under consideration allows us to calculate χ in a rather rigorous way and to investigate theoretically its variation with the droplet and film radii. Equations [5.1] and [5.3] can be used to calculate χ from the thermodynamic film radius and thickness determined by exploiting the procedure described in subsection 2.2 (see also Table 1). However, instead of Eqs. [5.1] and [5.3], we used an expression derived by Kralchevsky and Ivanov (27),

$$\chi = r_c\int_0^{\infty}\left[\left(\frac{\gamma\sin^2\phi}{x\cos\phi}\right) - \left(\frac{\gamma\sin^2\phi}{x\cos\phi}\right)^{id}\right]dx, \qquad [5.7]$$

which is more accurate for numerical processing. The first term of the integrand corresponds to the actual shape of the interface with smooth transition between film and meniscus, while the second one (with index id) corresponds to the idealized case of planar film with contact angle. In principle the two approaches are physically equivalent but that based on Eqs. [5.1] and [5.3] is much more sensitive towards inaccuracies in the numerical procedure, while the second (Eq. [5.7]) does not suffer from such disadvantages (see Ref. (27) for discussion).

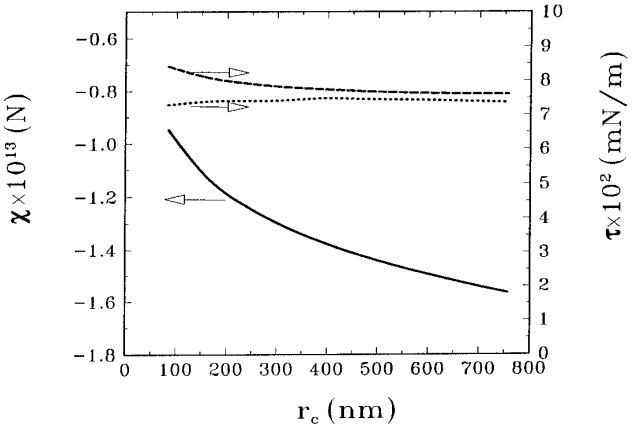

FIG. 8. Plot of the line tension χ (full curve), τ_c (dashed curve), and τ_e (dotted curve) as functions of the film radius. The remaining parameters are the same as those in Table 1.

In Fig. 8 we plot the dependence of χ on the film radius (the solid curve). The parameters of the droplets are the same as in Fig. 2 except the droplet radius which is varied from 1 μm to 10 μm. (The effect of gravity is neglected in these calculations, although it may become important for the larger droplets.) One sees from Fig. 8 that χ is negative; i.e., it tends to increase the film radius and contact angle in the numerical approach. It is a monotonically decreasing function of the film (and droplet) radius. The magnitude of χ is about 10^{-13} N and changes twice when the film radius is varied from 84 to 757 nm. These low values of the line tension mean small difference between the model and real shapes in the considered system and are about one order of magnitude less compared to those reported by de Feijter and Vrij (42). This can be explained by (i) the small size of the droplets studied, (ii) the absence of any outer force, and (iii) the equilibrium configuration (no dynamic effects are present).

Although the effect of χ on the equilibrium configuration of the doublet is detectable for micron size droplets, it is not very substantial. For instance, if the contribution of the line tension χ is neglected in Eq. [5.3], the three-phase contact angle and the film radius (calculated from Eqs. [3.2], [5.1]–[5.3]) for droplets of radius $a = 2$ μm would be $\alpha_c = 4.24°$ and $r_c = 147.8$ nm instead of the values 4.64° and 161.9 nm quoted in Table 1. One sees that these values are the same as those obtained by the model approach (26)—see Table 1. Hence, the effect of χ on the total interaction energy slightly changes the values of the film radius and contact angle. For larger droplets the *relative* contribution of the line tension is even less important. However, it can

be more pronounced for smaller droplets. The quantitative evaluation of this contribution for submicrometer droplets is not possible in the framework of the present model as explained in subsection 2.2.

One should note that the simpler model from Ref. (26) fails to predict the value of χ. Indeed, the combination of Eqs. [5.1], [5.3] from the present study and Eq. [9] from Ref. (26) gives (keeping the leading terms)

$$\gamma^{f} \approx \gamma^{l} \cos \alpha_e [1 + O(r_e^4/a^4)]. \quad [5.8]$$

(Note that the van der Waals contribution is incorporated in $f(h)$ in the present study, while in Ref. (26) it was considered separately.) One can conclude from this consideration that the effect of χ is probably responsible for the difference between the film radii calculated from the two approaches—see Table 1.

For the system under consideration, the transversal tension, τ, plays a very important role because it ensures the mechanical equilibrium of the doublet of droplets. As demonstrated in Fig. 6b, the interaction in the film region is predominantly repulsive. The value of τ is determined mostly from the attractive interaction between the curved surfaces surrounding the planar film. In Fig. 8 we plot the dependence of the line tension τ_c (as calculated from the numerical approach) on the film radius (the dashed curve). One sees from the figure that τ is almost constant when varying the film (or droplet) radius.

Contrary to the case of the line tension χ, the transversal tension, τ can be calculated by using the simple model described in Section 2.1. If we introduce the model droplet shape in Eq. [5.5] and replace the thermodynamic radius, r_c, with the film radius from the simple model, r_e, one obtains

$$\tau_e = -\frac{1}{r_e}\int_{r_e}^{\infty} \Pi(x) x\, dx \approx -\frac{a}{r_e}\int_{h}^{\infty} \Pi(H) dH = -\frac{a}{r_e} f(h), \quad [5.9]$$

where we have used the fact that in the film region $\Pi = P_c$ and the remaining surface is assumed to be spherical (see also Eq. [2.16]). However, according to Eq. [9] in Ref. (26), in equilibrium $f(h)$ can be expressed as

$$f(h_e) = -\gamma^{l} \frac{r_e^2}{a^2} = -\gamma^{l} \sin^2 \alpha_e. \quad [5.10]$$

From Eqs. [5.9] and [5.10] one obtains the following expression for the transversal tension, τ_e, in the framework of the model approach:

$$\tau_e = \gamma \sin \alpha_e. \quad [5.11]$$

The values calculated from Eq. [5.11] are plotted in Fig. 8 with a dotted line. One sees from the figure that the predictions of the approximate expression [5.11] are in a very good agreement with the exact values calculated from the real shape of the droplets.

At the end of this section we discuss briefly the theoretical approach previously developed by Churaev *et al.* (43) in the framework of the present consideration. These authors gave the first description of the shape of two interacting deformable droplets. Essentially, their method is very similar to ours (solving of the augmented Laplace equation). Still several differences can be outlined: (i) Churaev *et al.* (43) neglected (for simplicity) the variation of the film surface tension with the film thickness (cf. Eq. [2.12]). (ii) The numerical calculations were based on a model disjoining pressure isotherm which does not take into consideration the specific long-range decay of the van der Waals interactions (43). (iii) The interaction energy of the droplets was not determined in Ref. (43). Since we are interested mostly in the influence of different factors on the interaction energy (see Ref. (29)) calculations with more realistic isotherm are appropriate. The verification of the model approach (26) performed in the present paper needs a standard as accurate as possible.

6. CONCLUSIONS

An approach for determination of the actual shape and interaction energy of a doublet of two deformable droplets is presented. It consists of numerical integration of the augmented Laplace equation which accounts for the interaction between the droplets. This procedure allows us to obtain the film radius, thickness, and contact angle, as well as the different contributions to the interaction energy. Some calculations for micrometer-sized droplets are performed and compared with a simpler model (20, 26), which assumes that the droplets have the shape of spherical segments separated by a planar film. It is shown that the results from the two approaches are in very good agreement in wide range of droplet sizes. Also, the numerical solution of Laplace equation is unapplicable for a doublet of submicrometer-sized droplets. Therefore, one should use the simpler model (26) in that region. A detailed analysis of the effect of different factors on the pair interaction energy and droplet deformation is presented in the second part of this study (29).

The line and transversal tensions are calculated by means of the two approaches and compared. The first quantity accounts for the difference in the numerically calculated and the postulated (spherical segments) shapes. The second quantity accounts for the interaction between the curved regions of the droplet surfaces surrounding the planar film. The consideration of the line and transversal tensions allows complete thermodynamic description of the system in the framework of the two approaches.

ACKNOWLEDGMENTS

This study was supported by the Bulgarian Ministry of Science and Higher Education. Useful discussions with Professor Ivan B. Ivanov and Dr. Peter A. Kralchevsky are gratefully acknowledged. We are also indebted to Ms. M. Paraskova for typing the manuscript.

REFERENCES

1. Verwey, E. J. W., and Overbeek, J. Th. G., ''Theory and Stability of Lyophobic Colloids.'' Elsevier, Amsterdam, 1948.
2. Derjaguin, B. V., Churaev, N. V., and Muller, V. M., ''Surface Forces.'' Plenum, Consultants Bureau, New York, 1987.
3. Derjaguin, B. V., ''Theory of Stability of Colloids and Thin Liquid Films.'' Plenum, Consultants Bureau, New York, 1989.
4. Israelachvili, J. N., ''Intermolecular and Surface Forces.'' 2nd ed., Academic Press, London, 1991.
5. Kralchevsky, P. A., Danov, K. D., and Ivanov, I. B., *in* ''Foams: Theory, Measurements and Applications'' (R. K. Prud'homme, Ed.). Elsevier, Amsterdam, in press.
6. Russel, W. B., Saville, D. A., and Schowalter, W. R., ''Colloidal Dispersions.'' Cambridge Univ. Press, Cambridge, UK, 1989.
7. Hadziioannou, G., Patel, S., Cranick, S., and Tirrell, M., *J. Am. Chem. Soc.* **108,** 2869 (1986).
8. Asakura, S., and Oosawa, F., *J. Chem. Phys.* **22,** 1255 (1954); *J. Polym. Sci.* **33,** 183 (1958).
9. Richetti, P., and Kekicheff, P., *Phys. Rev. Lett.* **68,** 1951 (1992); Parker, J. L., Richetti, P., Kekicheff, P., and Sarman, S., *Phys. Rev. Lett.* **68,** 1955 (1992).
10. Aronson, M. P., *Langmuir* **5,** 494 (1989).
11. Ivanov, I. B., and Dimitrov, D. S., *in* ''Thin Liquid Films'' (I. B. Ivanov, Ed.) Chap. 8. Dekker, New York, 1988.
12. Ivanov, I. B., *Pure Appl. Chem.* **52,** 1241 (1980).
13. Ivanov, I. B., Dimitrov, D. S., Somasundaran, P., and Jain, R. K., *Chem. Eng. Sci.* **44,** 137 (1985).
14. Traykov, T. T., and Ivanov, I. B., *Int. J. Multiphase Flow* **3,** 471 (1977).; Traykov, T. T., Manev, E. D., and Ivanov, I. B., *Int. J. Multiphase Flow* **3,** 485 (1977).
15. Zhang, X., and Davis, R. H., *J. Fluid Mech.* **230,** 479 (1991).
16. Yiantsios, S. G., and Davis, R. H., *J. Colloid Interface Sci.* **144,** 412 (1991).
17. Aronson, M. P., and Princen, H., *Nature* **286,** 370 (1980); Aronson, M. P., and Princen, H., *Colloids Surf.* **4,** 173 (1982).
18. Hofman, J. A. M. H., and Stein, H. N., *J. Colloid Interface Sci.* **147,** 508 (1991).
19. Denkov, N. D., Kralchevsky, P. A., Ivanov, I. B., and Vassilieff, C. S., *J. Colloid Interface Sci.* **143,** 157 (1991).
20. Danov, K. D., Petsev, D. P., Denkov, N. D., and Borwankar, R., *J. Chem. Phys.* **99,** 7179 (1993).
21. Klahn, J. K., Agterof, W. G. M., van Voorst Vader, Groot, R. D., and Graenweg, F., *Colloids Surf.* **65,** 161 (1992).
22. Hamaker, H. C., *Physica* **4,** 1058 (1937).
23. Derjaguin, B. V., *Kolloid-Z.* **69,** 155 (1934).
24. Danov, K. D., Denkov, N. D., Petsev, D. N., and Borwankar, R., *Langmuir* **9,** 1731 (1993).
25. Smoluchowski, M., *Phys. Z.* **17,** 557, 785 (1916); *Z. Phys. Chem. (Leipzig)* **92,** 129 (1917).
26. Denkov, N. D., Petsev, D. N., and Danov, K. D., *Phys. Rev. Lett.* **71,** 3226 (1993).
27. Kralchevsky, P. A., and Ivanov, I. B., *Chem. Phys. Lett.* **121,** 111 (1985); *ibid* **121,** 116 (1985).
28. Ivanov, I. B., and Kralchevsky, P. A., *in* ''Thin Liquid Films'' (I. B. Ivanov, Ed.), Chap. 2. Dekker, New York, 1988; Nikolov, A. D., Kralchevsky, P. A., Ivanov, I. B., and Dimitrov, A. S., *AIChE Symp. Ser.* 252, **82,** 82 (1986).
29. Petsev, D. N., Denkov, N. D., and Kralchevsky, P. A., *J. Colloid Interface Sci.*, **176,** 201 (1995).
30. Dolan, A. K., and Edwards, S. F., *Proc. R. Soc. London, A* **337,** 509 (1974).
31. Ploehn, H. J., and Russel, W. B., *Adv. Chem. Eng.* **15,** 137 (1990).
32. Alexander, S. J., *Physique* **38,** 983 (1977); de Gennes, P. G., *Adv. Colloid Interface Sci.* **27,** 189 (1987).
33. Nikolov, A. D., and Wasan, D. T., *J. Colloid Interface Sci.* **133,** 1 (1989); Nikolov, A. D., Kralchevsky, P. A., Ivanov, I. B., and Wasan, D. T., *J. Colloid Interface Sci.* **133,** 13 (1989).
34. Nikolov, A. D., Wasan, D. T., Denkov, N. D., Kralchevsky, P. A., and Ivanov, I. B., *Prog. Colloid Polym. Sci.* **82,** 87 (1990); Wasan, D. T., Nikolov, A. D., Kralchevsky, P. A., and Ivanov, I. B., *Colloids Surf.* **67,** 139 (1992).
35. Kralchevsky, P. A., and Denkov, N. D., *Chem. Phys. Lett.* **240,** 385 (1995).
36. Bergeron, V., and Radke, C. J., *Langmuir* **8,** 3020 (1992).
37. Bibette, J., Roux, D., and Nallet, F., *Phys. Rev. Lett.* **65,** 2470 (1990); Bibette, J., Roux, D., and Pouligny, B., *J. Phys. II France* **2,** 401 (1992).
38. Danov, K. D. *et al.*, to be published.
39. de Feijter, J. A., *in* ''Thin Liquid Films'' (I. B. Ivanov, Ed.), Chap. 1. Dekker, New York, 1988.
40. Rusanov, A. I., *J. Colloid Interface Sci.* **53,** 20 (1975).
41. Ivanov, I. B., and Toshev, B. V., *Colloid Polym. Sci.* **253,** 558 (1975); *ibid* **253,** 593 (1975).
42. de Feijter, J. A., and Vrij, A., *J. Electroanal. Chem.* **37,** 9 (1972).
43. Churaev, N. V., Starov, V. M., and Derjaguin, B. V., *J. Colloid Interface Sci.* **89,** 16 (1982); Churaev, N. V., and Starov, V. M., *J. Colloid Interface Sci.* **103,** 301 (1985); Starov, V. M., *Adv. Colloid Interface Sci.* **39,** 147 (1992).
44. Ivanov, I. B., Nikolov, A. D., Kralchevsky, P. A., and Denkov, N. D., *J. Colloid Interface Sci.* **134,** 294 (1990).
45. Nikolov, A. D., Kralchevsky, P. A., and Ivanov, I. B., *J. Colloid Interface Sci.* **112,** 132 (1986).
46. Ivanov, I. B., Kralchevsky, P. A., Dimitrov, A. S., and Nikolov, A. D., *Adv. Colloid Interface Sci.* **39,** 77 (1992).
47. Dimitrov, A. S., Nikolov, A. D., Kralchevsky, P. A., and Ivanov, I. B., *J. Colloid Interface Sci.* **151,** 462 (1992).
48. Gajdos, and Neumann, A. W., *J. Colloid Interface Sci.* **120,** 76 (1987); Li, D., Cheng, P., and Neumann, A. W., *Adv. Colloid Interface Sci.* **39,** 347 (1992).
49. Platikanov, D., Nedyalkov, M., Scheludko, A., and Toshev, B. V., *J. Colloid Interface Sci.* **121,** 100 (1988).